# Sonochemistry of Surfactants in Aqueous Solutions: An EPR Spin-Trapping Study

**Joe Z. Sostaric* and Peter Riesz***

*Contribution from the Radiation Biology Branch, National Cancer Institute, National Institutes of Health, Bethesda, Maryland 20892*

*Received April 2, 2001. Revised Manuscript Received June 26, 2001*

**Abstract:** The surfactant properties of solutes play an important role in the sonochemistry and sonoluminescence of aqueous solutions. Recently, it has been shown, for relatively low molecular weight surfactants, that these effects can be correlated with the Gibbs surface excess of the solute. In the present study we investigate whether this correlation is valid for relatively high molecular weight surfactants and the mechanisms of surfactant decomposition during sonolysis. Sonolysis of argon-saturated aqueous solutions of nonvolatile surfactants [*n*-alkanesulfonates, *n*-alkyl sulfates, *n*-alkylammoniopropanesulfonates (APS), and poly(oxyethylenes) (POE)] was investigated by EPR and spin-trapping with 3,5-dibromo-4-nitrosobenzenesulfonate. Secondary carbon radicals ($-\dot{C}H-$), formed by abstraction reactions, were observed for all surfactants that were sonicated. The yield of primary carbon ($-\dot{C}H_2$) and methyl ($\dot{C}H_3$) radicals that are formed by pyrolysis is greatest for the zwitterionic (i.e., APS) and nonionic surfactants (i.e., POE). The yield of ($-\dot{C}H-$) radicals was measured following sonolysis of *n*-alkyl anionic surfactants [sodium pentanesulfonate (SPSo), sodium octanesulfonate (SOSo), sodium octyl sulfate (SOS), and sodium dodecyl sulfate (SDS)]. In the concentration range of 0−0.3 mM, the $-\dot{C}H-$ radical yield increases in the order SDS ≈ SOS ≈ SOSo > SPSo. At higher concentrations, a plateau in the maximum ($-\dot{C}H-$) radical yield is reached for each surfactant, which follows the order SPSo > SOS ≈ SOSo > SDS; i.e., the radical scavenging efficiency increases with decreasing *n*-alkyl chain length. A similar trend was observed for the $\dot{C}H_3$ yield following sonolysis of a homologous series of *n*-alkyl APS surfactants. The results show that the Gibbs surface excess of certain nonvolatile surfactants does not correlate with the extent of decomposition following sonolysis in aqueous solutions. Instead, the decomposition of surfactants depends on their chemical structure and their ability to equilibrate between the bulk solution and the gas/solution interface of cavitation bubbles.

## Introduction

Sonodynamic therapy is a promising new modality for cancer treatment based on the synergistic effect on cell killing by a combination of certain chemicals (sonosensitizers) and ultrasound. The effectiveness of sonodynamic therapy has been demonstrated in cell studies[1−4] and in tumor-bearing animals.[2,4−6] It has been proposed that the mechanism of cell killing involves the sonochemical decomposition of the sonosensitizer in the presence of oxygen and the formation of alkoxyl and peroxyl radicals which create oxidative stress at the cell membrane, eventually resulting in cell death.[7] The initial step in cell killing, i.e., the decomposition of the sonosensitizer, appears to be dependent on the ability of these nonvolatile, surface active molecules to accumulate at the gas/solution interface of cavitation bubbles,[7] which are produced during ultrasonic irradiation. We have investigated the yield and type of radicals formed following the sonolysis of nonvolatile, relatively long *n*-alkyl chain surfactants in aqueous solutions as a model for the mechanisms of accumulation and decomposition of sonosensitizers at the gas/solution interface of cavitation bubbles.

Sonochemistry, the initiation or enhancement of chemical activity by ultrasound, occurs due to a process known as cavitation, the formation, growth, and collapse of gas/vapor filled microbubbles in liquids. Discrete flashes of light are also associated with the collapse of these microbubbles, a phenomenon known as sonoluminescence. The process of bubble growth, which occurs over tens of microseconds, is followed by the sudden collapse of the bubble in the space of a few microseconds.[8] The widely accepted "hot spot" theory predicts that there is little time during bubble collapse for any significant heat or mass transfer to occur between the interior of the bubble and the surrounding liquid.[9,10] Hence, the almost adiabatic collapse of bubbles in solution results in the formation of small, localized regions of extremely high temperature (≈4300−5200 K)[11,12] and pressure (1000 atm),[13] surrounded by a hot shell,

* Corresponding authors. E-mail: J.Z.S., sostarij@mail.nih.gov; P.R., sono@helix.nih.gov.

(1) Yumita, N.; Nishigaki, R.; Umemura, K.; Umemura, S. *Jpn. J. Cancer Res.* **1990**, *81*, 304−308.
(2) Harrison, G. H.; Balcer-Kubiczek; Eddy, H. A. *Int. J. Radiat. Biol.* **1991**, *59*, 1453−1466.
(3) Kessel, D.; Jeffers, R.; Fowlkes, J. B.; Cain, C. *Int. J. Radiat. Biol.* **1994**, *66*, 221−228.
(4) Yumita, N.; Nishigaki, R.; Sakata, I.; Umemura, S. *Jpn. J. Cancer Res.* **2000**, *91*, 255−260.
(5) Yumita, N.; Umemura, S.; Nishigaki, R. *In Vivo* **2000**, *14*, 425−429.
(6) Yumita, N.; Nishigaki, R.; Umemura, S. *J. Cancer Res. Clin. Oncol.* **2000**, *126*, 601−606.
(7) Mišík, V.; Riesz, P. *Ann. N.Y. Acad. Sci.* **2000**, *899*, 335−348.
(8) Suslick, K. S. *Sci. Am.* **1989**, *260*, 80−86.
(9) Noltingk, B. E.; Neppiras, E. A. *Proc. Phys. Soc. B* **1950**, *63B*, 674−685.
(10) Neppiras, E. A.; Noltingk, B. E. *Proc. Phys. Soc. B* **1951**, *64B*, 1032−1038.
(11) Suslick, K. S.; Hammerton, D. A.; Cline R. E., Jr. *J. Am. Chem. Soc.* **1986**, *108*, 5641−5642.
(12) Didenko, Y. T.; McNamara, W. B., III; Suslick, K. S. *J. Phys. Chem. A* **1999**, *103*, 10783−10788.

10.1021/ja010857b CCC: $20.00 
Published on Web 10/10/2001

an initially liquid region which is heated to a maximum temperature of approximately 1900 K.[11] It has also been proposed that the hot, initially liquid zone is formed following the injection of jets or droplets of surrounding liquid into the bubble during the final stages of collapse.[14]

When the process of cavitation occurs in an aqueous argon-saturated solution, the water molecules in the bubble undergo thermal homolysis to produce the primary radical species, hydrogen atoms (·H) and hydroxyl radicals (·OH).[15,16] Thus, the creation of hot spots and ·H and ·OH radicals are the processes by which chemical reactivity is initiated when aqueous solutions are exposed to ultrasound. There are three regions where chemical reactions can occur during sonolysis: (I) the core of the hot spot; (II) the hot shell surrounding the hot spot; (III) the bulk solution at ambient temperature, where radicals formed in regions I and II may diffuse to react with solute molecules. It has been shown that the volatility and surface activity of an organic solute determine its fate during sonolysis, as described below.

Nonvolatile, hydrophilic organic solutes were shown to undergo abstraction reactions in the bulk solution.[17−19] On the other hand, volatile organic solutes evaporate into growing bubbles and exist at relatively high concentrations in the core of the hot spot. These molecules undergo pyrolysis reactions[20−23] and readily quench sonoluminescence.[12,24,25] Nonvolatile surfactants have been shown to readily accumulate in the hot shell surrounding the hot spot,[26−28] where they may undergo pyrolysis and readily scavenge the primary radicals. Volatile surfactants may also evaporate into the bubble and thus decompose in the hot spot.

The hot spot has a lifetime of less than 1 $\mu$s;[8] thus, there is no time for any surfactant to move from the bulk of the solution into the hot shell. Instead, the final concentration of surfactant in the hot shell will be determined by the ability of the surfactant to adsorb at the gas/solution interface of the cavitating bubble as it grows in size.

When a surfactant is added to water, the surface tension ($\gamma$) decreases as the surfactant begins partitioning at the gas/solution interface, until an equilibrium surface tension ($\gamma_{eq}$) is reached. When equilibrium is attained, a measure of the two-dimensional concentration of surfactant at the gas/solution interface can be obtained using the Gibbs surface excess ($\Gamma_{eq}$).[29a] For a neutral surfactant $\Gamma_{eq}$ can be calculated using the Gibbs−Duhem equation:

$$\Gamma_{eq} = -\frac{1}{kT}\frac{d\gamma_{eq}}{d(\ln C_{surfactant})} \quad (1)$$

Where $C_{surfactant}$ is the bulk concentration of surfactant. For ionic surfactants, the equation becomes more complex as the adsorption of counterions must also be taken into consideration.[29b] For a homologous series of surfactants, as the chain length is increased, $\Gamma_{eq}$ will also be larger for a certain bulk surfactant concentration.[29c]

Indeed, a quantitative relationship was shown to exist between the efficiency of dissolution of $MnO_2$ particles during sonolysis in aqueous solutions and $\Gamma_{eq}$ of a homologous series of *n*-alcohols, from ethanol to pentan-1-ol.[30] Furthermore, Grieser and co-workers conducted a number of studies on the effects of relatively short *n*-alkyl chain surfactants, such as aliphatic alcohols, amines, and carboxylic acids, and relatively small aromatic compounds, such as aniline and phenol, on sonochemistry[31,32] and multibubble sonoluminescence[31,33−35] observed in aqueous solutions. Again, the particular effect being observed was found to depend on $\Gamma_{eq}$.

However, the adsorption of *n*-alkyl surfactants at the gas/solution interface from the bulk solution is a time-dependent process[36] and is affected by a number of parameters, including the *n*-alkyl chain length of the surfactant. In the current study we evaluate the mechanisms of the sonochemical decomposition of *n*-alkyl surfactants (of varying alkyl chain length; see Table 1) and the general applicability $\Gamma_{eq}$ to predict the ability of different classes of surfactants to adsorb at the gas/solution interface of bubbles in an ultrasonic field.

## Experimental Section

**Materials.** $H_2O_2$ (30%) was supplied by Fisher Scientific, and the stock solution concentration was determined from the extinction coefficient of $H_2O_2$ at 230 nm (81 $M^{-1}$ $cm^{-1}$). 3,5-Dibromo-4-nitrosobenzenesulfonic acid-$d_2$ (DBNBS-$d_2$) was obtained from Dr. Miles Chedekel's Melanin Laboratories. Sodium *n*-octyl sulfate (SOS, 99%) was supplied by Lancaster, and sodium dodecyl sulfate (SDS, ≥99%), by Fluka. All other reagents were purchased from the Sigma Chemical Co. and include 4-hydroxy-2,2,6,6-tetramethylpiperidinyloxy (TEMPOL), 3,5-dibromo-4-nitrosobenzenesulfonic acid (DBNBS), sodium 1-pentanesulfonic acid (SPSo), sodium 1-octanesulfonic acid (SOSo), sodium 1-decanesulfonic acid (SDeSo), *n*-octyl-*N*,*N*-dimethyl-3-ammonio-1-propanesulfonate ($C_8$APS), *n*-decyl-*N*,*N*-dimethyl-3-ammonio-1-propanesulfonate ($C_{10}$APS), *n*-dodecyl-*N*,*N*-dimethyl-3-ammonio-1-propanesulfonate ($C_{12}$APS), poly(oxyethylene-8-decyl ether) ($C_{10}E_8$)

(13) Suslick, K. S.; McNamara, W. B., III; Didenko, Y. In *Sonochemistry and Sonoluminescence*; Crum, L. A., Mason, T. J., Reisse, J. L., Suslick, K. S., Eds.; Nato ASI Series C: Mathematical and Physical Sciences; Kluwer Academic Publishers: Dordrecht, The Netherlands, 1999; Vol. 524, pp 191−204.
(14) Suslick, K. S.; Didenko, Y.; Fang, M. M.; Hyeon, T.; Kolbeck, K. J.; McNamara, W. B., III; Mdleleni, M. M.; Wong, M. *Philos. Trans. R. Soc. London A* **1999**, *357*, 335−353.
(15) Makino, K.; Mossoba, M. M.; Riesz, P. *J. Am. Chem. Soc.* **1982**, *104*, 3537−3539.
(16) Makino, K.; Mossoba, M. M.; Riesz, P. *J. Phys. Chem.* **1983**, *87*, 1369−1377.
(17) Gutiérrez, M.; Henglein, A.; Fischer, C.-H. *Int. J. Radiat. Biol.* **1986**, *50*, 313−321.
(18) Hart, E. J.; Henglein, A. *Radiat. Phys. Chem.* **1988**, *32*, 11−13.
(19) Tauber, A.; Schuchmann, H.-P.; von Sonntag, C. *Ultrason. Sonochem.* **2000**, *7*, 45−52.
(20) Krishna, C. M.; Lion, Y.; Kondo, T.; Riesz, P. *J. Phys. Chem.* **1987**, *91*, 5847−5850.
(21) Riesz, P.; Kondo, T.; Carmichael, A. J. *Free Rad. Res. Commun.* **1993**, *19*, S45−S53.
(22) Drijvers, D.; De Baets, R.; De Visscher, A.; Van Langenhove, H. *Ultrason. Sonochem.* **1996**, *3*, S83−S90.
(23) Tauber, A.; Mark, G.; Schuchmann, H.-P.; von Sonntag, C. *J. Chem. Soc., Perkin Trans. 2* **1999**, 1129−1135.
(24) Sehgal, C.; Steer, R. P.; Sutherland, R. G.; Verrall, R. E. *J. Phys. Chem.* **1977**, *81*, 2618−2620.
(25) Sehgal, C.; Sutherland, R. G.; Verrall, R. E. *J. Phys. Chem.* **1980**, *84*, 388−395.
(26) Henglein, A.; Kormann, C. *Int. J. Radiat. Biol.* **1985**, *48*, 251−258.
(27) Henglein, A.; Gutiérrez, M. *J. Phys. Chem.* **1988**, *92*, 3705−3707.
(28) Alegria, A. E.; Lion, Y.; Kondo, T.; Riesz, P. *J. Phys. Chem.* **1989**, *93*, 4908−4913.
(29) Hunter, R. J. *Foundations of colloid science*; Clarendon Press: Oxford, U.K., 1995; Vol. 1: (a) pp 246−254; (b) pp 256−257; (c) pp 254−255; (d) pp 19−20; (e) pp 574−576.
(30) Sostaric, J. Z.; Mulvaney, P.; Grieser, F. *J. Chem. Soc., Faraday Trans.* **1995**, *91*, 2843−2846.
(31) Barbour, K.; Ashokkumar, M.; Caruso, R. A.; Grieser, F. *J. Phys. Chem. B* **1999**, *103*, 9231−9236.
(32) Caruso, R. A.; Ashokkumar, M.; Grieser, F. *Colloids Surf., A* **2000**, *169*, 219−225.
(33) Ashokkumar, M.; Hall, R.; Mulvaney, P.; Grieser, F. *J. Phys. Chem. B* **1997**, *101*, 10845−10850.
(34) Ashokkumar, M.; Mulvaney, P.; Grieser, F. *J. Am. Chem. Soc.* **1999**, *121*, 7355−7359.
(35) Ashokkumar, M.; Vinodgopal, K.; Grieser, F. *J. Phys. Chem. B* **2000**, *104*, 6447−6451.
(36) Eastoe, J.; Dalton, J. S. *Adv. Colloid Interface Sci.* **2000**, *85*, 103−144.

**Table 1.** Surfactants Used in This Study Showing Their Abbreviation, Structure, Classification, and Critical Micelle Concentrations (cmc)

| | Surfactant | Abbreviation | Structure: Tail | Structure: Head | CMC[a] (mM) |
|---|---|---|---|---|---|
| Sulfate or Sulfonate Head Group (Anionic) | Sodium 1-pentane sulfonic acid | SPSo | $C_5H_{11}$ | $OSO_2^-Na^+$ | 990[b] |
| | Sodium 1-octane sulfonic acid | SOSo | $C_8H_{17}$ | $OSO_2^-Na^+$ | 144[b] |
| | Sodium 1-decane sulfonic acid | SDeSo | $C_{10}H_{21}$ | $OSO_2^-Na^+$ | - |
| | Sodium n-octyl sulfate | SOS | $C_8H_{17}$ | $OSO_3^-Na^+$ | 133[b] |
| | Sodium dodecyl sulfate | SDS | $C_{12}H_{25}$ | $OSO_3^-Na^+$ | 8.2[b] |
| APS Head Group (Zwitterionic) | n-octyl-N,N,-dimethyl-3-ammonio-1-propane sulfonate | $C_8$APS | $C_8H_{17}$ | $^+N(CH_3)_2(CH_2)_3OSO_2^-$ | 330[c] |
| | n-decyl-N,N,-dimethyl-3-ammonio-1-propane sulfonate | $C_{10}$APS | $C_{10}H_{21}$ | $^+N(CH_3)_2(CH_2)_3OSO_2^-$ | 25-40[c] |
| | n-dodecyl-N,N,-dimethyl-3-ammonio-1-propane sulfonate | $C_{12}$APS | $C_{12}H_{25}$ | $^+N(CH_3)_2(CH_2)_3OSO_2^-$ | 2-4[c] |
| POE Head Group (Non-Ionic) | Polyoxyethelene-8-decyl ether | $C_{10}E_8$ | $C_{10}H_{21}$ | $(OCH_2CH_2)_8OH$ | 1.0[d] |
| | Polyoxyethelene-8-lauryl ether | $C_{12}E_8$ | $C_{12}H_{25}$ | $(OCH_2CH_2)_8OH$ | - |

[a] The presence of DBNBS in solution will affect the absolute value of the cmc. Nevertheless, these values give a good qualitative description of the surface activity of each surfactant. [b] Reference 57. [c] Obtained from the Calbiochem Biochemicals data sheet for zwitterionic surfactants. [d] Reference 58.

and poly(oxyethylene-8-lauryl ether) ($C_{12}E_8$). Table 1 lists the surfactants used in this study, along with their structure and critical micelle concentrations (cmc). All solutions were made with Milli-Q filtered water (conductivity $<10^{-6}$ S cm$^{-1}$ and surface tension of 72.0 mN m$^{-1}$ at 25 °C). Glassware was washed using Extran 300 detergent supplied by Electron Microscopy Sciences.

**Sonolysis Experiments.** Stock solutions were prepared in glassware that was soaked for 2−3 h in Extran 300 and 1 h in concentrated nitric acid and then rinsed thoroughly with Milli-Q water. Unless otherwise indicated, samples (1 mL) were placed in Kimble disposable 13 × 100 mm borosilicate glass culture tubes (supplied by Thomas Scientific) and fixed in the center of a sonication bath (either Bransonic model 1210, 47 kHz, or model 1510, 42 kHz). The sample solution was sealed using a "suba seal" (supplied by Aldrich) and bubbled with argon gas for 5 min. Argon gas was passed over the surface of the solution during sonolysis. The temperature of the sonication bath water was maintained at 20 ± 1 °C during sonolysis. Under these conditions, 5 min of sonolysis of a Fricke dosimeter solution[37] resulted in an absorbance change at 302 nm of 1.10 ± 0.06 (47 kHz) or 0.70 ± 0.03 (42 kHz) in a 1 cm quartz cell.

Occasionally, bubbling argon gas through certain surfactant solutions at high concentrations resulted in excessive foaming. For this reason, certain solutions were saturated with argon by the "freeze/thaw" method. To test the reliability of this gassing procedure, a 1 mM solution of SDS was argon saturated, using either the standard or freeze/thaw methods, and the $-{}^{\cdot}CH-$ radical yield measured following 5 min of sonolysis. On average, the yield varied by less than 5% between the two methods.

**$H_2O_2$−UV Photolysis Experiments.** Hydroxyl radicals were formed by the photolysis (270 ± 10 nm) of $H_2O_2$. The sample solution containing the surfactant, DBNBS (8.2 mM), and $H_2O_2$ (0.069 mM to 0.69 mM) was placed in the EPR standard quartz flat (60 × 10 × 0.25 mm) cell and irradiated continuously in the cavity of the EPR spectrometer at room temperature with a Schoeffel 1000 W xenon lamp coupled to a Schoeffel grating monochromator. Photolysis was continued until the EPR spectrum reached a maximum intensity. No radicals could be spin-trapped during photolysis (270 nm) of surfactants in the absence of $H_2O_2$, indicating that the radicals trapped by DBNBS were formed via radical abstraction reactions with hydroxyl radicals and not by direct photolysis of the surfactant.

**Table 2.** Hyperfine Coupling Constants (Hfccs) of Radicals Spin-Trapped Using DBNBS during Sonolysis and Photolysis Experiments of Aqueous Surfactant Solutions[a]

| | | Hfccs (G) | | | |
|---|---|---|---|---|---|
| | | sonolysis | | photolysis | |
| surfactant | radical | $a_N$ | $a(\beta)_H$ | $a_N$ | $a(\beta)_H$ |
| SPSo | $R_1{}^{\cdot}CHR_2$ | 14.16 | 8.13 | 14.25 | 8.20 |
| SOSo | $R_1{}^{\cdot}CHR_2$ | 14.25 | 8.17 | 14.13 | 8.1 |
| SOS | $R_1{}^{\cdot}CHR_2$ | 14.23 | 8.18 | 14.21 | 8.13 |
| SDS | $R_1{}^{\cdot}CHR_2$ | 14.24 | 8.21 | 14.21 | 8.23 |
| $C_{10}E_8$ | $R_1{}^{\cdot}CHR_2$ | 14.05 | 8.21 | 14.17 | 8.17 |
| | ${}^{\cdot}CH_2R$ | 13.89 | 13.26(2) | | |
| | ${}^{\cdot}CH_3$[b] | 14.45 | 13.50(3) | | |
| $C_8$APS | $R_1{}^{\cdot}CHR_2$ | 14.26 | 8.29 | 14.11 | 8.33 |
| $C_{12}$APS | $R_1{}^{\cdot}CHR_2$ | 14.22 | 8.33 | 14.24 | 8.37 |

[a] Methyl (${}^{\cdot}CH_3$) radicals were trapped for all surfactants following sonolysis and had the same hfccs as those shown in the table for $C_{10}E_8$. [b] The hfcc from the hydrogen atoms in the meta position of the benzene ring of DBNBS was 0.8 G.

**EPR Measurements.** Surfactant sample solutions containing either DBNBS (8.2 mM) or DBNBS-$d_2$ (2.7 mM) were removed immediately following sonolysis and transferred into a standard EPR flat quartz cell. EPR spectra were recorded at room temperature on a Varian E-9 X-band spectrometer with 100 kHz modulation frequency. The EPR software, "EPRDAP", written by Dr. P. Kuppusamy (U.S. EPR Inc., Clarksville, MD) was used for the acquisition, analysis, and simulation of EPR spectra. Absolute radical yields were determined by comparing the EPR spectra of surfactants following sonolysis with the EPR spectra of a stable nitroxide (TEMPOL). It should be noted that errors are introduced by the conversion of relative to absolute spin adduct yields. However, this conversion does not affect the relative radical yields on which the conclusions of this study are based. DBNBS-$d_2$ was used to determine the methyl radical yields following sonolysis since the hydrogen coupling of the nondeuterated analogue is removed, resulting in better resolution of the spectrum and a more accurate determination of methyl radical yields. The typical instrument settings for the quantitative measurements of the spin adducts of DBNBS and DBNBS-$d_2$ were the following: microwave power, 20 mW; modulation amplitude, 1 G; time constant, 0.128 s; scan speed, 50 G/min. The decay of the radical adducts of interest was insignificant during the measurement time.

## Results

**Sonochemical Decomposition of Surfactants in Aqueous Solution.** EPR spectra of the spin adducts of DBNBS consist of a triplet due to the splitting of the spin resonance line from the unpaired electron into three lines by the $^{14}N$ nucleus. These three lines are further split depending on the number of hydrogen nuclei that are attached to the α-carbon atom of the adduct.[38] From the splitting pattern produced by the radical adduct, the type of organic radical that was spin-trapped, i.e., tertiary (${}^{\cdot}CR_3$), secondary ($-{}^{\cdot}CH-$), primary ($-{}^{\cdot}CH_2$), or methyl (${}^{\cdot}CH_3$) radical, can readily be determined. The sonolysis of anionic, POE, and APS surfactants resulted in the production of carbon-centered radicals which were spin-trapped using DBNBS. Table 2 lists the type of radicals spin-trapped and their nitrogen ($a_N$) and hydrogen ($a_H$) hyperfine coupling constants.

(37) Spinks, J. W. T.; Woods, R. J. *An Introduction to Radiation Chemistry*, 3rd ed.; Wiley-Interscience: New York, 1990.

(38) Krishna, C.; Kondo, T.; Riesz, P. *J. Phys. Chem.* **1989**, *93*, 5166−5172.

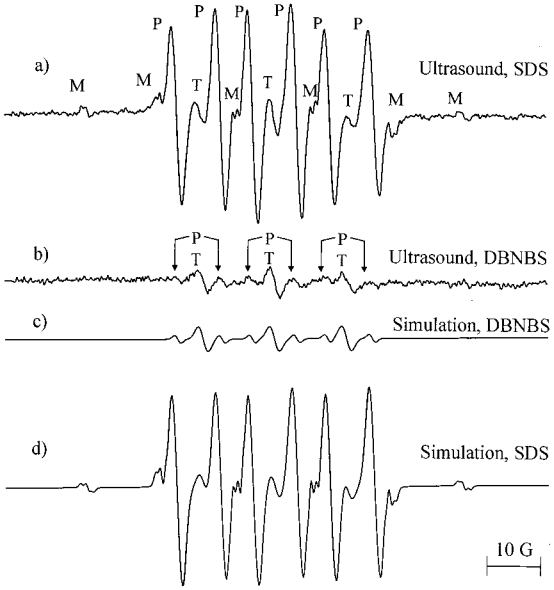


**Figure 1.** EPR spectrum following the 47 kHz sonolysis of (a) SDS (3 mM) in the presence of DBNBS (8.2 mM) and (b) DBNBS (8.2 mM). The lines in the spectra represent either methyl (M), primary (P), or tertiary (T) carbon radical spin adducts. Computer simulations of the spectra are shown for (c) the DBNBS spectrum and (d) the SDS spectrum. Conditions: argon-saturated solutions; $T = 20 \pm 1$ °C; time of sonolysis = 5 min.

The EPR spectrum observed when a SDS solution (3 mM) was sonicated (47 kHz) for 5 min under argon and in the presence of DBNBS (8.2 mM) is shown in Figure 1a. The main feature of the spectrum is the presence of three doublets (labeled P) which are due to the primary ($-\dot{C}H-$) radical adduct. A small yield of methyl radicals (labeled M) is also observed. Three more lines are present in the spectrum (labeled T), which are attributed to the decomposition of DBNBS during sonolysis. This is shown in Figure 1b, where a spectrum of a DBNBS solution, sonicated for 5 min under the same conditions gave the same three lines[39] (labeled T) as those observed in Figure 1a. The spectrum in Figure 1b was simulated as a combination of a tertiary carbon radical with $a_N = 13.28$ G and a $-\dot{C}H-$ radical with splitting of $a_N = 13.9$ G and $a_H = 8.3$ G (Figure 1c).

The spectrum in Figure 1a was simulated as a $-\dot{C}H-$ and $\dot{C}H_3$ radical component with the coupling constants shown in Table 2 for SDS. To this was added the simulation of the underlying DBNBS background spectrum (Figure 1c) to yield the spectrum shown in Figure 1d. There is a good correlation between the observed (Figure 1a) and the simulated (Figure 1d) spectra following the sonolysis of a SDS solution. Spectra were collected for a series of anionic surfactants, including SOS, SOSo, and SPSo, following sonolysis under the same conditions as those in the experiments shown in Figure 1a. These spectra were similar to that observed for SDS (see Table 2 for coupling constants).

The EPR spectra following the sonolysis of zwitterionic ($C_8$APS, $C_{10}$APS, $C_{12}$APS) and nonionic ($C_{10}E_8$, $C_{12}E_8$) surfactants were measured. The $C_8$APS spectrum in Figure 2a was simulated in Figure 2b as $-\dot{C}H-$ (labeled P) and $\dot{C}H_3$ (labeled M) radicals with the splitting constants shown in Table 2. The yield of secondary $-\dot{C}H_2$ radicals (labeled S) was too small to simulate accurately. $C_{10}$APS and $C_{12}$APS yielded similar spectra (not shown) to the one observed for $C_8$APS. The $C_{10}E_8$ spectrum (Figure 3a) was simulated as a contribution of $-\dot{C}H-$ (labeled P), $-\dot{C}H_2$ (labeled S), and $\dot{C}H_3$ (labeled M) radicals (Figure 3b; see Table 2 for coupling constants). The $C_{12}E_8$ spectrum (not shown) resembled that of $C_{10}E_8$.

(39) The intensities of these lines are small in comparison to $-\dot{C}H-$ lines observed following sonolysis of surfactant solutions, and there is little overlap between the two. Thus, the role of DBNBS decomposition can be neglected.

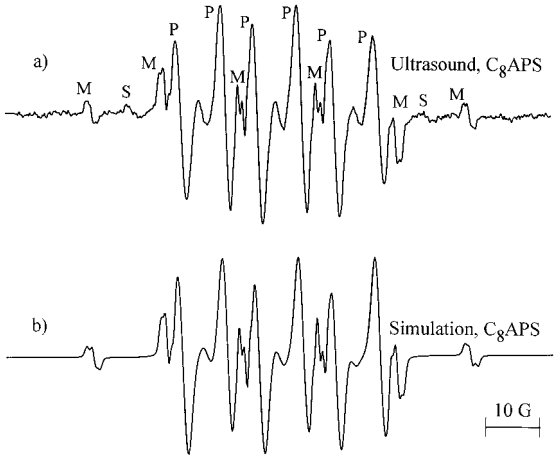


**Figure 2.** (a) EPR spectrum following the 47 kHz sonolysis of $C_8$-APS (10 mM) in the presence of DBNBS (8.2 mM). Conditions: argon-saturated solutions; $T = 20 \pm 1$ °C; time of sonolysis = 5 min. The lines in the spectra represent either methyl (M), primary (P), or secondary (S) carbon radical spin adducts. (b) Computer simulation of the spectrum in (a). Note that the underlying secondary carbon radical has not been simulated; however, the small contribution of the DBNBS decomposition products (Figure 1c) has been added to the simulation.

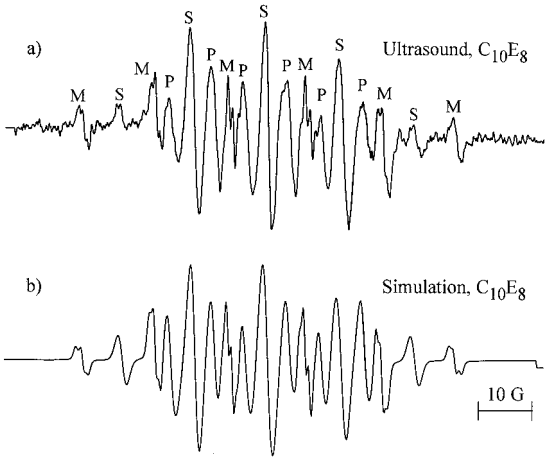


**Figure 3.** (a) EPR spectrum following the 47 kHz sonolysis of $C_{10}E_8$ (0.3 mM) in the presence of DBNBS (8.2 mM). Conditions: argon-saturated solutions; $T = 20 \pm 1$ °C; time of sonolysis = 5 min. The lines in the spectra represent either methyl (M), primary (P), or secondary (S) carbon radical spin adducts. Shown in (b) is a computer simulation of spectrum a. The underlying DBNBS contribution (Figure 1c) has been added to this spectrum.

The UV (270 nm) photolysis in the presence of $H_2O_2$ (0.069 and 0.69 mM) of all of the surfactants examined in this study was investigated, and in each case, $-\dot{C}H-$ radicals were observed but no $\dot{C}H_3$ radicals were detected (e.g., Figure 4). A barely detectable yield of $-\dot{C}H_2$ radicals was observed for the anionic and APS surfactants following $H_2O_2$ photolysis. An example of this is shown for the case of SOSo (Figure 4b). It should be noted that the $-\dot{C}H-$ radical coupling constants observed following $H_2O_2$ photolysis of surfactants are approximately equal to the coupling constants of the $-\dot{C}H-$ radicals spin-trapped during sonolysis of the same surfactant solutions (Table 2).

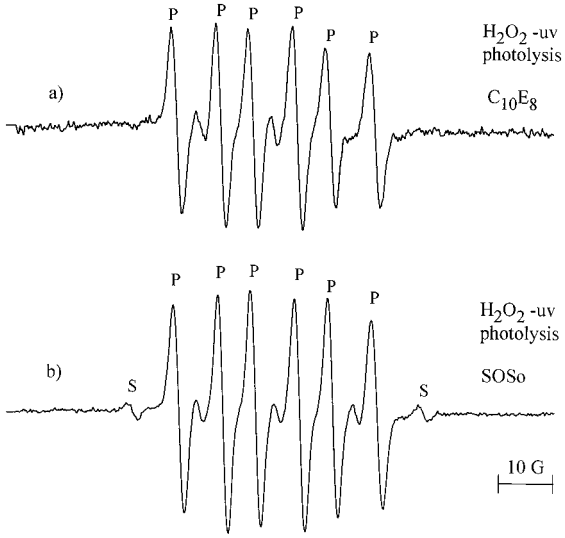


**Figure 4.** EPR spectrum of the radicals spin-trapped by DBNBS (8.2 mM) during the $H_2O_2$−UV photolysis of (a) $C_{10}E_8$ (1 mM) in the presence of 0.69 mM $H_2O_2$ and (b) SOSo (30 mM) in the presence of 0.069 mM $H_2O_2$. The lines in the spectra are due to primary (P) or secondary (S) carbon radical spin adducts. Low-intensity lines in the spectra are due to the small contribution of DBNBS decomposition.

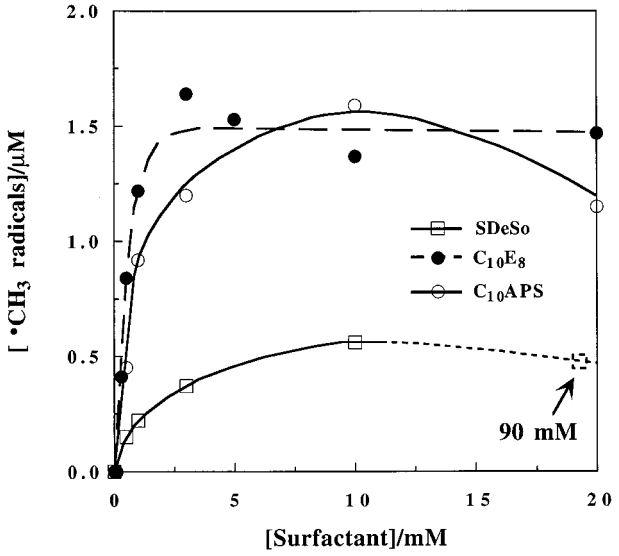


**Figure 5.** Effect of surfactant concentration and headgroup structure on the methyl radical yield observed following sonolysis in the presence of DBNBS-$d_2$ (2.7 mM). The freeze/thaw method was used to saturate the solutions with argon. Sonolysis was conducted for 5 min at 42 kHz and $T = 20 \pm 1$ °C.

The effect of sonolysis of three surfactants with a $C_{10}$ *n*-alkyl chain length, possessing different headgroup structures (i.e., APS, POE, or sulfonate), was investigated by determining the methyl radical yield (Figure 5). The methyl radical yield is much higher for $C_{10}E_8$ and $C_{10}$APS than it is for the anionic surfactant, SDeSo. These results imply that the structure of the headgroup of these surfactants has a significant effect on the yield of pyrolysis radicals following sonolysis.

**Comparison of *n*-Alkyl Chain Length on Radical Yields.** The yields of −•CH− radicals for $C_8$APS (1 mM), $C_{12}$APS (0.2 mM), and SOSo (1 mM) as a function of sonication time are shown in Figure 6. The yield of −•CH− radical adduct is directly proportional to the time of sonolysis (up to 6 min). Hence, under the current experimental conditions spin-trapping

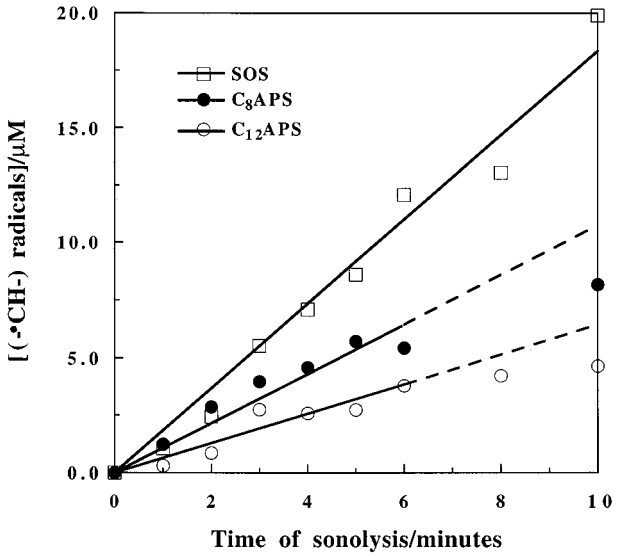


**Figure 6.** Concentration of −•CH− radicals as a function of the time of sonolysis of various surfactant solutions. Conditions: DBNBS, 8.2 mM; argon-saturated; $T = 20 \pm 1$ °C.

and EPR can be used as a quantitative measure of radical scavenging during ≤6 min of sonolysis of *n*-alkyl surfactant solutions.

The effect of surfactant concentration (0−3 mM) on the yield of −•CH− radicals for SPSo, SOSo, SOS, and SDS is shown in Figure 7a. In the low concentration range (<0.3 mM) the −•CH− radical yield increases in the order SPSo < SOSo ≈ SOS ≈ SDS. For SDS, SOS, and SOSo, there appears to be little dependence of the −•CH− radical yield on the chain length of the surfactants in this low concentration range. At higher surfactant concentrations (1−10 mM) all of the surfactants eventually reached a limiting value in −•CH− radical yield, as shown in Figure 7b (note that all surfactants are well below their respective critical micelle concentrations, Table 1). The height of this plateau value for −•CH− radical production increased in the order SDS < SOS ≈ SOSo < SPSo. This is opposite to the order that would have been expected, had −•CH− radical formation been determined by $\Gamma_{eq}$ of the surfactants. A similar trend in radical adduct formation was observed after the sonolysis of a homologous series of APS surfactants.

The $•CH_3$ radical adduct yield following the sonolysis of a series of APS surfactants of varying *n*-alkyl chain length, in the 0−10 mM concentration range, is presented in Figure 8a. Clearly, the maximum $•CH_3$ radical yield is obtained during the sonolysis of the shortest chain surfactant, $C_8$APS, followed by $C_{10}$APS and finally $C_{12}$APS, which gives the lowest $•CH_3$ radical yield. When the surfactant concentrations were increased beyond the CMC ($C_{12}$APS = 2−4 mM, $C_{10}$APS = 25−40 mM), the $•CH_3$ radical yield decreased to zero (Figure 8b). In the case of $C_8$APS, the cmc was not reached (cmc = 330 mM) and the $•CH_3$ radical yield remained constant over the concentration range from 10 to 60 mM.

## Discussion

**Mechanistic Aspects of Radical Formation during Surfactant Sonolysis.** In argon-saturated aqueous solutions, the formation of •H and •OH radicals in the hot spot (reaction 2) can lead to a number of other reactions. In the absence of any solutes, these primary radical species can recombine in the hot spot or in the hot shell (reactions 3−5). In the presence of

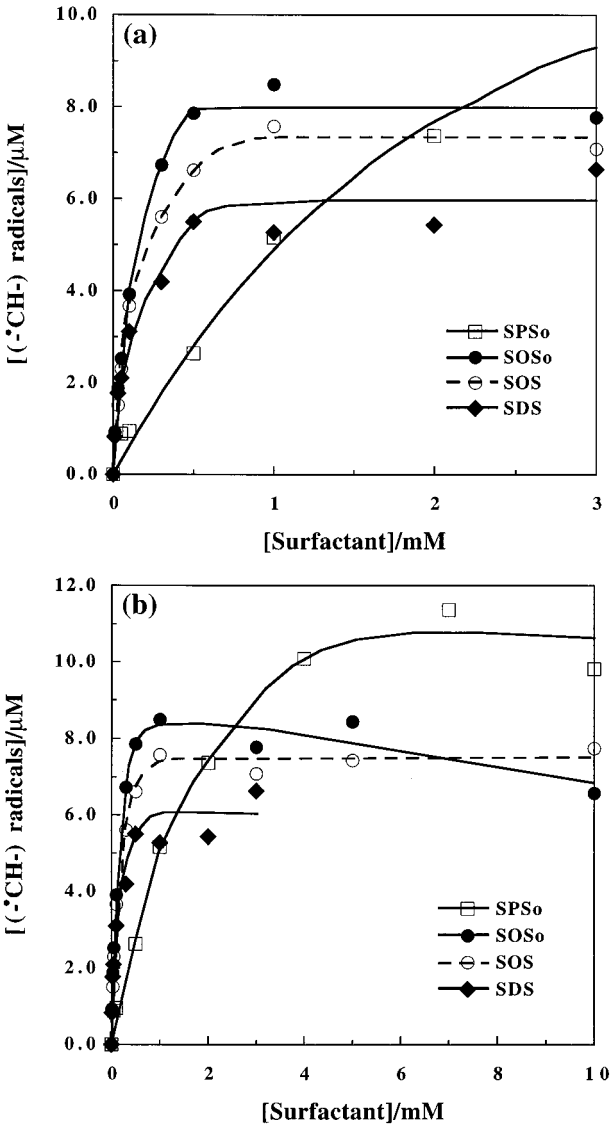


**Figure 7.** $-{}^{\cdot}CH-$ radical concentration following 5 min of sonolysis of a homologous series of *n*-alkyl chain anionic surfactants in the concentration range of (a) 0−3 mM and (b) 0−10 mM. DBNBS (8.2 mM). Conditions: argon-saturated; $T = 20 \pm 1$ °C.

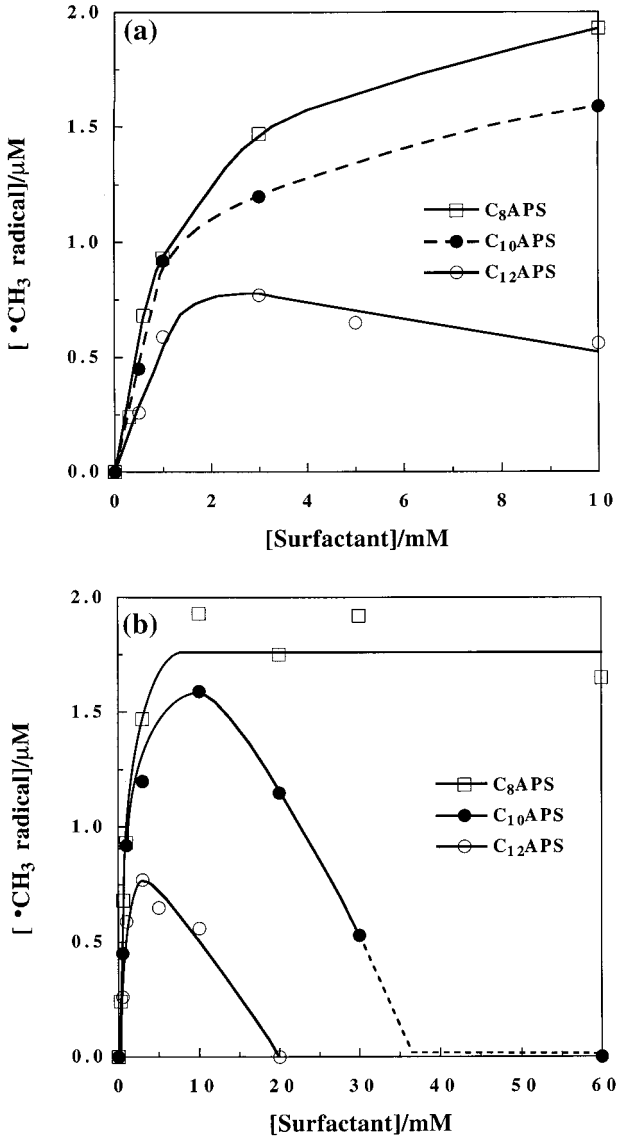


**Figure 8.** ${}^{\cdot}CH_3$ radical concentration following 5 min of sonolysis of a homologous series of *n*-alkyl chain APS surfactants in the concentration range of (a) 0−10 mM and (b) 0−60 mM. The freeze/thaw method was used to saturate the solutions with argon. Sonolysis was conducted for 5 min at 42 kHz, $T = 20 \pm 1$ °C, and in the presence of DBNBS-$d_2$ (2.7 mM).

organic solutes in the bulk solution, ·OH and ·H radicals may react with the organic solute (RH) to produce secondary radical species (R·), reaction 6. Considerably fewer hydrogen atoms than ·OH radicals are available for reaction in the bulk solution:[7,40]

$$H_2O \xrightarrow{)))))} {}^{\cdot}OH + {}^{\cdot}H \quad (2)$$

$${}^{\cdot}H + {}^{\cdot}OH \rightarrow H_2O \quad (3)$$

$${}^{\cdot}H + {}^{\cdot}H \rightarrow H_2 \quad (4)$$

$${}^{\cdot}OH + {}^{\cdot}OH \rightarrow H_2O_2 \quad (5)$$

$$RH + {}^{\cdot}OH\ ({}^{\cdot}H) \rightarrow R^{\cdot} + H_2O\ (H_2) \quad (6)$$

Surfactant molecules exist at relatively high concentrations in the hot shell of the hot spot and can scavenge a proportion of the primary radical species in this region, thus competing with the primary radical recombination processes (reactions 3−5). Primary radical scavenging results in the abstraction of hydrogen atoms from the alkyl chain of all surfactants and in the case of the APS and POE surfactants from the $-CH_2-$ units in the headgroup (see Table 1) to produce $-{}^{\cdot}CH-$ radicals. Furthermore, there is a possibility that a hydrogen atom can be abstracted from the terminal carbon atom on the alkyl chain of the surfactant. However, this does not occur to any appreciable degree since no $-{}^{\cdot}CH_2$ radicals were detected following the sonolysis of the anionic surfactants (e.g., Figure 1) and either a very low yield of or no $-{}^{\cdot}CH_2$ radicals were observed when $H_2O_2$ photolysis was conducted in the presence of any of the surfactants (e.g., Figure 4).

The above discussion indicates that the majority of $-{}^{\cdot}CH_2$ and all of the ${}^{\cdot}CH_3$ radicals are formed as a result of pyrolysis reactions. Since the surfactant molecules in the current study are nonvolatile, their pyrolysis takes place in the hot shell surrounding the hot spot. The alkyl chain of any of the surfactants can pyrolyse either by thermal homolysis of C−C

(40) Henglein, A. In *Advances in Sonochemistry*; Mason, T. J., Ed.; JAI Press Ltd.: London, 1993; Vol. 3, pp 17−83.

**Table 3.** Range of Static Dielectric Constants ($\epsilon$) and the Phase of Water in the Temperature Range of 100 to 600 °C and Particular Pressure Ranges Where the Negative log of the Ion Product of Water ($-\log K_w$) Is Less Than 14

| temp (°C) | pressure range (MPa) | range of $-\log K_w$[a] | range of $\epsilon$[b] | phase |
|---|---|---|---|---|
| 100 | 0.1014−100 | 12.265−11.96 | 55.50−58.67 | liquid |
| 150 | 1.0−100 | 11.638−11.29 | 44.08−47.33 | liquid |
| 200 | 5.0−100 | 11.289−10.86 | 34.93−38.33 | liquid |
| 250 | 5.0−100 | 11.191−10.60 | 27.05−31.07 | liquid |
| 300 | 10.0−100 | 11.406−10.50 | 20.22−25.10 | liquid |
| 350 | 20.0−100 | 12.30−10.54 | 13.96−20.08 | liquid |
| 400 | 50.0−100 | 11.88−10.77 | 12.04−15.80 | supercritical |
| 450 | 50.0−100 | 13.74−11.19 | 6.69−12.13 | supercritical |
| 500 | 75.0−100 | 13.01−11.81 | <10 | supercritical |
| 600 | 100 | 13.40 | 5.06 | supercritical |

[a] Reference 59. [b] Reference 60.

bonds or by $\beta$-scission of a C−C bond, following the abstraction of a hydrogen atom, similar to the thermal cracking of alkanes.[41a] It was shown that the structure of the surfactant has a marked effect on the yield of pyrolysis radicals observed following sonolysis (Figure 5). This result is discussed in detail in the following two sections.

**Decomposition of APS Surfactants.** The decomposition of the APS surfactant may occur by a Hofmann-type elimination reaction on a quaternary amine.[42] In the case of $C_8$APS, this will result in the formation of a 1-octene or a tertiary amine, as shown in reaction 7:

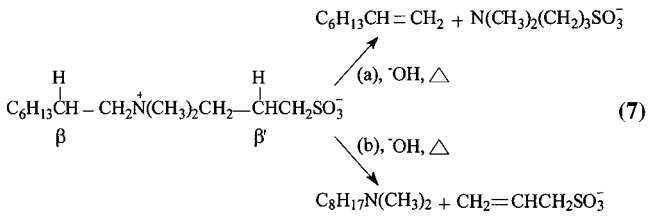

(7)

The tail, rather than the headgroup of $C_8$APS, is more likely to be eliminated because the $-CH_2SO_3^-$ group is more electron releasing compared to the $C_6H_{13}-$ group. Hence, the $\beta'$-proton is less acidic than the $\beta$-proton and elimination would tend to follow pathway a in reaction 7.

Generally, the Hofmann-type elimination reaction is catalyzed by hydroxide ions at the relatively moderate temperatures of approximately 100 °C.[41b] Even though the experiments in this study were conducted in the absence of base, there may be a number of characteristics of the hot shell which would be conducive to the Hofmann-type elimination of the APS surfactants.

At the temperatures and pressures of the hot shell, regions of superheated and possibly supercritical water exist where the ion product of water ($K_w$) is greater than that observed under ambient conditions at neutral pH (i.e., $K_w = 10^{-14}$), as shown in Table 3. Thus, in the particular regions of the hot shell where the temperature increases from 100 to 600 °C, the concentration of $^-$OH ions may vary from between 0.1 to 5.6 $\mu$M. More importantly, the dielectric constant of superheated water decreases considerably as the temperature increases above 100 °C under pressures where the phase remains either liquid or supercritical (Table 3). As the dielectric constant decreases, so too does the hydration number of ions. Interestingly, it has been shown that dehydrated ions possessing high charge density, such as $^-$OH ions, become highly reactive when the Hofmann-type elimination reaction is conducted in nonpolar liquids.[43]

The 1-octene that is produced (reaction 7) is highly hydrophobic and will prefer to adsorb to and eventually be drawn into a new bubble(s) that is formed in the region of the original hot spot, rather than dissolving in the aqueous phase. A similar process was proposed by Grieser and co-workers to explain the quenching of sonoluminescence by organic additives.[34] The 1-octene will undergo pyrolysis in the core of the hot spot, with a greater efficiency than the original surfactant in the hot shell, resulting in an increased methyl radical yield. Similar processes would also occur for $C_{10}$APS and $C_{12}$APS.

**Decomposition of POE Surfactants.** It was shown (Figure 4a) that no $-^{\cdot}CH_2$ radicals are formed during the $H_2O_2$–UV photolysis of $C_{10}E_8$. Furthermore, following sonolysis no $-^{\cdot}CH_2$ radicals were observed from ionic surfactants (e.g., Figure 1) and a barely detectable yield of $-^{\cdot}CH_2$ radicals were formed from APS surfactants (e.g., Figure 2). Thus, it follows that $-^{\cdot}CH_2$ radicals are formed during the decomposition of the headgroup of $C_{10}E_8$ (Figure 3), since all three surfactant families possess alkyl chains. Methyl radicals may be produced following the pyrolysis of smaller, hydrophobic components in a similar way to that described above for the APS surfactant.

The decomposition of the POE headgroup of $C_{10}E_8$ (and $C_{12}E_8$) might occur by pyrolysis. However, during pyrolysis in the hot shell at temperatures of up to 1900 K, the difference in bond dissociation enthalpy between a C−C bond in the alkyl chain of the surfactant (e.g., $C_3H_7$–$CH_3$ = 356.5 kJ/mol)[44] and a C−O bond in the headgroup of the surfactant (e.g., $C_3H_7$–$OCH_3$ = 338.9 kJ/mol)[44] may not be large enough to account for the increase in $^{\cdot}CH_3$ and $-^{\cdot}CH_2$ radicals observed for the POE surfactants, in comparison to the anionic surfactants.

Alternatively, decomposition of the POE headgroup may be due to radical attack followed by $\beta$-scission of the C−C bonds in the headgroup, as described earlier for the decomposition of the alkyl chain of the surfactants. The POE headgroup may be more prone to $^{\cdot}OH$ attack compared to the alkyl chain of $C_{10}E_8$ (or $C_{12}E_8$), since it is known that hydroxyl radicals selectively abstract hydrogen atoms from the α-alkoxyalkyl positions of ethers.[45,46] The mechanism of decomposition can occur via two pathways, as shown reaction 8:

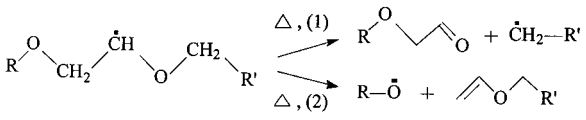

(8)

$-^{\cdot}CH_2$ radicals are spin-trapped by DBNBS, while $R-O^{\cdot}$ cannot be spin-trapped by DBNBS. Furthermore, the products produced in reaction 8 may undergo further decomposition in new bubbles, as explained earlier for the sonolysis of APS surfactants. It is plausible that $\beta$-scission of the POE headgroup of $C_{10}E_8$ and $C_{12}E_8$ (reaction 8) occurs at a faster rate than $\beta$-scission of the *n*-alkyl chain of the anionic surfactants, leading to higher yields of $-^{\cdot}CH_2$ and $^{\cdot}CH_3$ radicals for the POE surfactants in comparison to the anionic surfactants.

However, why $\beta$-scission of the POE headgroup is favored in comparison to the alkyl chain is not immediately clear since

(41) Fieser, L. F.; Fieser, M. *Advanced Organic Chemistry*; Reinhold Publishing: New York, 1961: (a) p 123; (b) p 509.
(42) March, J. *Advanced Organic Chemistry: Reactions, Mechanisms and Structure*, 4th ed.; John Wiley and Sons: New York, 1992; pp 1015−1016.
(43) Maia, A. *Pure Appl. Chem.* **1995**, *67*, 697−702.
(44) Wentrup, C. *Reactive Molecules: The neutral reactive intermediates in organic chemistry*; John Wiley and Sons: New York, 1984; p 28.
(45) Schuchmann, M. N.; von Sonntag, C. *J. Phys. Chem.* **1982**, *86*, 1995−2000.
(46) Janik, I.; Ulanski, P.; Rosiak, J. M.; von Sonntag, C. *J. Chem. Soc., Perkin Trans. 2* **2000**, 2034−2040.

it is known that surfactant will adsorb at the gas/solution interface of the bubble with the hydrophobic alkyl chain pointing toward the hot interior of the bubble and the hydrophilic headgroup remaining completely solvated.[29d] There are a number of hypotheses to explain why the temperature to which the POE headgroup is exposed during and following collapse of the bubble may be similar to that experienced by the alkyl chain.

First, because of the slight hydrophobicity of the ethylene units of the POE headgroup, it can approach a parallel orientation to the gas/solution interface.[47] Furthermore, in a study modeling the dynamic surface tension of $C_iE_j$ type surfactants,[48] it has been shown that the parallel orientation of the POE headgroup is approached during the early stages of the adsorption process. At longer adsorption times, the headgroup attains a perpendicular orientation to the interface.[48] The results of the current study show that equilibrium adsorption at the gas/solution interface of cavitation bubbles is far from being attained for long chain surfactants (see later), suggesting that the POE headgroups are orientated parallel to the interface.

Secondly, if liquid droplets or jets of liquid can be injected from the bubble interface, into the interior of the bubble,[14] then the decomposition of the all parts of the surfactant molecule takes place at the similar temperatures in these superheated, initially liquid droplets.

**Radical Reactions following the Sonolysis of Aqueous Surfactant Solutions.** The dependence of the maximum $-{}^{\cdot}CH-$ radical yield on the concentration of the anionic surfactants (Figure 7b) could be explained in terms of the rates of reaction of the primary radicals for the different surfactants in bulk solution (reaction 6). However, the rate of reaction of ${}^{\cdot}OH$ radicals with a series of *n*-alkyl surfactants (in units of $10^9$ $dm^3\ mol^{-1}\ s^{-1}$) follows the order SDS (8.0) > SOS (6.5) > sodium hexyl sulfate (2.5) > sodium butyl sulfate (1.0).[49] Thus, the rate of reaction increases with increasing alkyl chain length, which is opposite to the trend observed for maximum $-{}^{\cdot}CH-$ radical yield (Figure 7b), which decreases with increasing chain length.

The secondary radical species ($R^{\cdot}$) produced (reaction 6) are either spin-trapped by DBNBS (reaction 9), can undergo radical−radical recombination (reaction 10) or can abstract a hydrogen atom from another surfactant molecule (reaction 11):

$$R^{\cdot} + \text{DBNBS} \rightarrow R-{}^{\cdot}\text{DBNBS} \quad (9)$$

$$R^{\cdot} + R^{\cdot} \rightarrow R_2 \quad (10)$$

$$R^{\cdot} + R'H \rightarrow RH + R'' \quad (11)$$

Figure 7 shows that the $-{}^{\cdot}CH-$ radical yield for anionic surfactants increases rapidly at low concentrations until a plateau value is attained. The observation that the $-{}^{\cdot}CH-$ radical yield remains constant over a surfactant concentration range of approximately 1−10 mM (Figure 7b) implies that reaction 11 does not compete significantly with reaction 9, in this concentration range. It is plausible that reaction 10 competes with the spin-trapping process (reaction 9), since the secondary carbon radical (${}^{\cdot}R$) may exist at relatively high concentrations in the hot shell. However, radical−radical recombination would be expected to be close to the diffusion controlled limit for all of the surfactants and would not account for the results observed in Figure 7.

It is conceivable that the spin-trapping rate (reaction 9) varies for different surfactants. This may explain the increasing yield of $-{}^{\cdot}CH-$ radicals at high surfactant concentrations as the chain length of the surfactant decreases (Figure 7b). However, even if this were the case during the spin-trapping of $-{}^{\cdot}CH-$ radicals, this would not explain why the methyl radical spin-trapping efficiency increased with decreasing chain length of APS surfactants (Figure 8a).

When methyl radicals are spin-trapped, reactions 9 and 10 will be independent of the surfactant systems studied, since the radical being spin-trapped is identical. Although the rate of reaction of methyl radicals with the different surfactants (reaction 11) will vary, it does not compete with reaction 9, since the methyl radical yield for $C_8$APS reaches a plateau and effectively remains constant as the concentration is increased from approximately 10 to 60 mM (Figure 8b). The sudden decrease in methyl radical yield for $C_{10}$APS and $C_{12}$APS at relatively high concentrations (Figure 8b) is due to the formation of micelles. A similar effect was observed by Alegria et al.[28] At concentrations above the critical micelle concentration (cmc), the bulk solution concentration of monomer surfactant remains constant.[29e] Thus, the amount of surfactant that can partition at the gas/solution interface also remains the same. There are several possible explanations for the decreasing methyl radical yield above the cmc. First, the spin-trap itself may partition at the interface of the micelle, thus decreasing the spin-trapping efficiency. Second, zwitterionic surfactants form spherical and rod-shaped micelles in solution[50] which will increase the viscosity of the system, thus decreasing inertial cavitation.[51]

**Adsorption of Surfactants at the Gas/Solution Interface of Cavitation Bubbles.** On the basis of the above discussion, it is proposed that the $-{}^{\cdot}CH-$ and ${}^{\cdot}CH_3$ radical yield is effectively determined by the ability of the homologous series of *n*-alkyl surfactants to accumulate at the gas/solution interface of cavitation bubbles. However, the results presented in Figures 7 and 8 are inconsistent with the idea that surfactants with a greater equilibrium surface activity accumulate at the gas/solution interface of cavitation bubbles with a greater efficiency.

The results of this study are in good agreement with those observed previously by multibubble sonoluminescence.[52] In the sonoluminescence study, aqueous solutions containing either SDS, SOS, SOSo, or SPSo were sonicated under argon gas at a frequency of 358 kHz and the sonoluminescence spectra were measured. The spectra showed an intense sodium atom emission band at concentrations as low as 0.4 mM, much lower than the concentrations of NaCl required to produce a sodium emission band (ca. 10−50 mM). The anionic surfactant that can partition at the gas/solution interface of the bubble to the greatest degree attracts a greater amount of sodium ions from the bulk solution to the bubble interface, from where sodium atom emission can occur following collapse of the bubble. In the multibubble sonoluminescence study,[52] the emission from excited sodium atoms was measured as a function of the bulk surfactant concentration and was found to follow the same profile as that observed for $-{}^{\cdot}CH-$ radical yield in this study; i.e., the maximum Na* emission intensity followed the order SPSo > SOS ≈ SOSo > SDS.

The current observations can be explained in terms of the dynamics of surfactant accumulation at the gas/solution interface

(47) Lu, J. R.; Thomas, R. K.; Penfold, J. *Adv. Colloid Interface Sci.* **2000**, *84*, 143−304.

(48) Ravera, F.; Liggieri, L.; Miller, R. *Colloids and Surf., A* **2000**, *175*, 51−60.

(49) Almgren, M.; Grieser, F.; Thomas, J. K. *J. Chem. Soc., Faraday Trans. 1* **1979**, *75*, 1674−1687.

(50) Israelachvili. *Intermolecular and Surface Forces*; Academic Press Limited: London, 1992; p 374.

(51) Flynn, H. G. In *Physical Acoustics 1 (Part B)*; Mason, W. P., Ed.; Academic Press Limited: New York, 1964; pp 57−172.

(52) Sostaric, J. Z. Interfacial Effects on Aqueous Sonochemistry and Sonoluminescence. Ph.D. Thesis, The University of Melbourne, 1999.

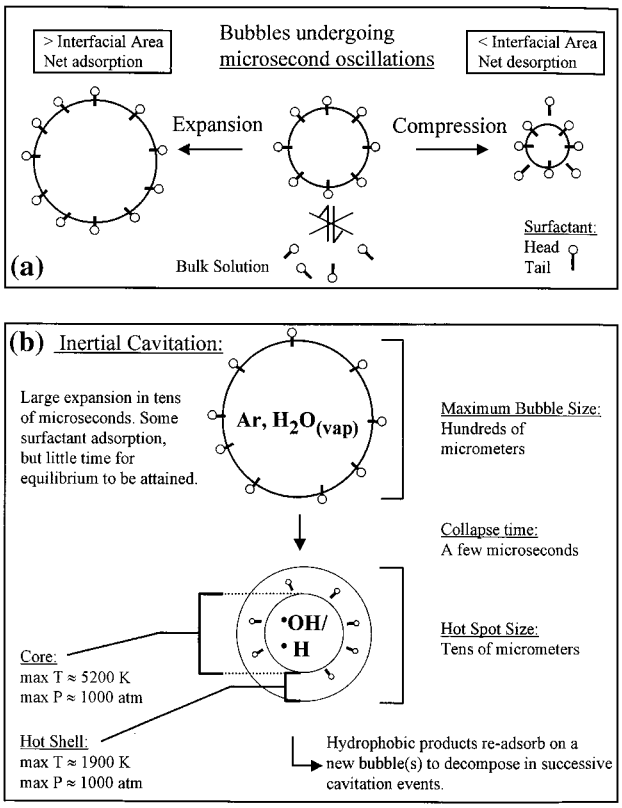


**Figure 9.** Diagram describing the adsorption of surfactant at the gas/solution interface of cavitation bubbles. (a) Surfactant in the bulk solution cannot equilibrate with that at the gas/solution interface of a stable cavitation bubble. (b) Surfactant accumulation at the interface of a rapidly growing bubble. Collapse is so fast that there is no time for surfactant to adsorb from the bulk solution to the bubble interface. The hot spot has a lifetime of less than 1 $\mu$s. The hot shell surrounding the hot spot is a region of superheated and possibly supercritical water, which is formed during the final stages of collapse. (Surfactant molecules, bubbles, and the hot spot are not drawn on a relative scale.)

of cavitation bubbles. When a new interface is formed, there is net diffusion of surfactant molecules from the bulk solution to a narrow region just below the interface (i.e., the subsurface),[36] so that equilibrium can be established again. On reaching the subsurface, the surfactant molecule may have to overcome a number of barriers to adsorption, including an increased surface pressure, less vacant sites in the interface for adsorption, and being in the correct orientation for adsorption to take place.[36] These barriers may result in any particular surfactant molecule not being able to adsorb, thereby back-diffusing into the bulk solution and increasing the overall time required for equilibrium to be established. In general, it is the combined effects of diffusion of surfactant from the bulk solution to the subsurface and the overcoming of barriers to adsorption from the subsurface to the interface that limit the rate of surfactant adsorption at the gas/solution interface.[36]

The interface of cavitation bubbles is either growing or contracting on a microsecond time scale,[53,54] which at 47 kHz is approximately 10−20 $\mu$s. Thus, there is either net adsorption (during bubble growth) or net desorption (during bubble compression) of surfactant (Figure 9a). Furthermore, the time scale of the bubble growth processes is too short compared to the length of time required for the relatively long-chain surfactants to equilibrate with the gas/solution interface of the bubble.

Fainerman et al.[55] studied the gas/solution adsorption dynamics of *n*-alkyl chain surfactants, possessing a sulfate headgroup. It was shown that a 2 mM solution of SDS reached equilibrium after more than 3 ms.[55] Furthermore, approximately 700 $\mu$s passed before the surface excess concentration of SDS reached 50% of $\Gamma_{eq}$.[55] These times are much longer than the period of bubble oscillations or the lifetime of transient cavities and will greatly effect the amount of surfactant that can accumulate at the gas/solution interface of cavitation bubbles.

An important factor that can determine the surfactant's ability to reach equilibrium at the gas/solution interface is the length of the hydrocarbon chain. Ferri and Stebe[56] considered the rate at which homologous series of surfactants could attain equilibrium between the bulk solution and the gas/solution interface, by comparing dynamic properties of surfactants with their equilibrium properties. Surfactants that have a higher equilibrium surface excess concentration ($\Gamma_{eq}$) at a particular bulk concentration will reduce the surface tension to the greatest degree at equilibrium.[56] However, these surfactants require longer times to equilibrate.[56] For the surfactants in our study, the trends in $\Gamma_{eq}$ for a given bulk concentration will follow the trend SDS > SOS ≈ SOSo > SPSo. Thus, in accordance with the conclusions of Ferri and Stebe,[56] the rate at which these molecules can adsorb at the gas solution interface follows the opposite trend. Furthermore, it was concluded that surfactants which are not very surface active equilibrate extremely rapidly.[56] The observations made in the current study showing that SPSo, with a cmc of 990 mM, has resulted in the greatest amount of primary radical scavenging at the gas/solution interface of cavitation bubbles fits with the conclusions that can be derived from a consideration of the dynamic surface tension properties of surfactants. Similar arguments can be made with regard to the accumulation of the APS surfactants at the gas/solution interface of cavitation bubbles.

## Conclusions

The processes leading to the sonochemical decomposition of nonvolatile surfactants are depicted in Figure 9. Bubbles are formed and then oscillate under the influence of the ultrasonic wave (Figure 9a) or undergo growth in less than one acoustic cycle followed by inertial collapse (Figure 9b). In this study it has been shown that $\Gamma_{eq}$ cannot describe adsorption of certain anionic and APS surfactants, possessing an *n*-alkyl chain greater than five carbon atoms, at the gas/solution interface of cavitation bubbles. The situation can arise where surfactants that are substantially less surface active under equilibrium conditions can more readily accumulate at the gas/solution interface of cavitation bubbles, at a particular bulk concentration, compared to surfactants with a greater equilibrium surface activity. Following bubble collapse (Figure 9b), all parts of the surfactant

(53) Neppiras, E. A. *Phys. Rep.* **1980**, *61*, 159−251.
(54) Young, F. R. *Cavitation*; McGraw-Hill: London, U.K., 1989; pp 38−186.
(55) Fainerman, V. B.; Makievski, A. V.; Miller, R. *Colloids Surf., A* **1994**, *87*, 61−75.
(56) Ferri, J. K.; Stebe, K. J. *Adv. Colloid Interface Sci.* **2000**, *85*, 61−97.
(57) Mukerjee, P.; Mysels, K. J. *Critical Micelle Concentrations of Aqueous Surfactant Systems*; U.S. Government Printing Office: Washington, DC, 1970; Vol. 36.
(58) Rosen, M. J. *Surfactants and Interfacial Phenomena*, 2nd ed.; Wiley-Interscience: New York, 1988.
(59) Franck, E. U. *J. Phys. Chem. Ref. Data* **1981**, *10*, 295−304.
(60) Archer, D. G.; Wang, P. M. *J. Phys. Chem. Ref. Data* **1990**, *19*, 371−411.

may, on average, be equally exposed to the high temperatures produced in the hot shell. This would facilitate chemical processes which would otherwise not be possible had the headgroup of the surfactant remained completely solvated in the bulk solution. The current study shows that consideration must be given to the mechanisms of decomposition and to the dynamics of accumulation of surfactants at the gas/solution interface of cavitation bubbles when interpreting the effect of surfactants on sonochemistry and sonoluminescence of aqueous solutions.

**Acknowledgment.** J.Z.S. was funded by a visiting fellowship from the Fogarty International Center, NIH. We wish to thank Professor M. M. Kreevoy of the Department of Chemistry, The University of Minnesota, for helpful discussions.

JA010857B